Solid-State NMR Characterization of Phenylbenzimidazolesulfonic Acid Coencapsulated with Cetyltrimethylammonium in Mesoporous Silica Materials

Raphaël Bongur,[†] Nicolas Marx,[†] Claire Marichal,*[,†] Bénédicte Lebeau,*[,†] and Philippe Guarilloff[‡]

Equipe Matériaux à Porosité Contrôlée, Institut de Science des Matériaux de Mulhouse, LRC CNRS 7228, Université de Haute-Alsace, ENSCMu, 3 rue Alfred Werner, 68093 Mulhouse Cedex, France, and Chanel PB Laboratory, 876 Centannial Avenue, Piscataway, New Jersey 08855

Received: July 24, 2009; Revised Manuscript Received: December 1, 2009

The hydrophilic molecule phenylbenzimidazolesulfonic acid (PBSA) has been coencapsulated with cetyltrimethylammonium chloride (CTAC), an amphiphilic surfactant, via an in situ method in a mesoporous silica matrix. The effect of coencapsulation on texture and structure of the mesoporous silica host has been studied by X-ray diffraction (XRD), transmission electron microscopy (TEM), nitrogen sorption experiments, and ^{29}Si magic-angle spinning (MAS) NMR spectroscopy. It was clearly observed that the presence of PBSA led to different characteristics compared to the reference MCM-41 type organized mesoporous silica (OMS), which suggests that the active molecules perturb the silica network formation. The encapsulation of the hydrophilic PBSA molecule was found to be stable in aqueous media, indicating that strong interactions exist between PBSA and its environment (surfactant and silica framework). ^{1}H−^{29}Si and ^{1}H−^{13}C MAS NMR experiments evidenced their spatial proximity and confirmed the presence of interaction between PBSA and both CTA^+ molecules and silanol of the silica framework. This NMR study gave an overall picture of the organic/inorganic interface.

1. Introduction

Organized mesoporous silica (OMS) materials have been attracting much interest since they were reported by Beck and co-workers.[1,2] Such materials—characterized by amorphous walls, highly ordered pore structure, large surface area (up to 1500 $m^2 \cdot g^{-1}$), and large pore diameter (10−300 Å) with a narrow pore-size distribution—are suitable for a wide range of applications. Recently, significant efforts have been devoted to make OMS as functional materials for specific applications. In particular, the narrow pore-size distribution and the large pore size of OMS confers upon them a high potential for inclusion chemistry.[3] For example, supports with large pores are of great interest for numerous catalytic applications that require the introduction of accessible catalytic centers such as ions,[4] metal clusters,[5] or metal complexes[6] into the pores. Another area of contemporary interest has been the incorporation of transition elements such as Ag to generate continuous metal "nanowires" within the pores.[7] Moreover, pores of OMS are used as nanoreactors for several applications such as olefin polymerization.[8] The pore structure is also used to synthesize mesoporous silica/polymer nanocomposites by inclusion and polymerization of monomers.[9] In relation to inclusion chemistry research area, there has been widespread interest concerning the use of such materials for encapsulation of organic molecules largely due to their relevance to medicine, pharmaceutics, agriculture, and cosmetic industries depending on the encapsulated molecules.[10,11] In particular, the encapsulation of sensitive organic molecules into inorganic matrices may improve their thermal stability[12] and photostability[13] or their solubility.[14] Several methods for encapsulating organic molecules into the pores of the hosts are suggested in the literature, including loading by sorption,[15−17] ion exchange,[18,19] and covalent grafting.[20−22] Recently, an interesting in situ encapsulation based on an original approach for the entrapment of different molecules in inorganic matrices was proposed.[23−25] It is easy to perform and has the advantage of immobilizing a high amount of these organic molecules, in an active and stable form.

In this work, the in situ encapsulation of phenylbenzimidazolesulfonic acid (PBSA) in mesoporous silica was performed for the first time. PBSA is a hydrophilic molecule widely used as a sunscreen agent,[26,27] which absorbs most efficiently in the 290−320 nm region (UV-B) of solar UV radiation. Such a molecule was already successfully occluded in inorganic matrices such as clays[28] or in organic hosts, such as cyclodextrin.[29] The main goal of encapsulation in these cases is to improve the photostability of the active molecule and to reduce human skin penetration.

As a first step toward those objectives, in situ encapsulation of PBSA molecules in mesoporous silica matrices was studied in particular by solid-state NMR. Indeed this technique has already provided relevant information about the localization of the guest molecules, the host−guest interactions,[30] and the mobility of the guest molecules that are of key importance for understanding the properties of such complex systems.[24,31,32]

It is interesting to note that the in situ encapsulation method leads to a more complicated system than the conventional postsynthesis encapsulation method, which consists in adsorption of active molecules, like ibuprofen,[33] within surfactant-free OMS matrices. Indeed, in the former case, three components must be taken into account, namely, the active molecule (PBSA), the cetyltrimethylammonium cationic surfactant (CTA^+), and the silica matrix.

* Corresponding authors: e-mail claire.marichal@uha.fr or benedicte.lebeau@uha.fr.
[†] Université de Haute-Alsace.
[‡] Chanel PB Laboratory.

10.1021/jp907051f
Published on Web 12/23/2009

This work is devoted to the study of the effect of in situ coencapsulation on the mesoporous silica host, the surfactant, and the active molecules (PBSA), not only by conventional characterization techniques such as X-ray diffraction (XRD), N_2 adsorption−desorption measurements, transmission electron microscopy (TEM), and thermal analyses but also by one- and two-dimensional (1D and 2D) ^{29}Si and ^{13}C solid-state magic-angle spinning (MAS) NMR spectroscopy.

2. Experimental Section

2.1. Materials Synthesis. The synthesis of CTA^+−PBSA coencapsulated material was accomplished according to the synthesis method of MCM-41 materials described by Voegtlin et al.,[34] with the use of cetyltrimethylammonium chloride (CTAC, 25 wt % in distilled water, Fluka) as a structure-directing agent, sodium silicate (SiNa, 10 wt % NaOH, 27 wt % SiO_2, Riedel-de-Haën) as silica source, NaOH (99 wt %, Riedel-de-Haën), and PBSA, purchased from DSM.

NaOH (1.4 g) was dissolved in 88.9 mL of distilled water. SiNa (13.3 g) was added to the previous solution and 4.8 g of PBSA was then dissolved in the mixture. After complete dissolution, 14.8 mL of CTAC solution was added. An immediate gelation was observed and the temperature of the mixture was increased to 323 K, in order to allow stirring. The starting molar ratio was 1 SiO_2:0.29 PBSA:0.19 CTAC:110.96 H_2O:0.58 NaOH. The mixture was stirred for 2 h at room temperature and 48.4 mL of HCl 1 M was added drop by drop, in order to adjust pH to 8.5. The mixture was transferred into closed polypropylene flask and left in an oven at 363 K for 24 h. After reaction, the solid was recovered by centrifugation at 11000*g* for 20 min in an Eppendorf 5804-R centrifuge, washed two times with distilled water, and dried overnight at 343 K.

For comparison purposes, a reference material was also synthesized by the same procedure, without introduction of PBSA. The starting molar ratio was 1 SiO_2:0.19 CTAC:110.96 H_2O:0.58 NaOH. In the reference and coencapsulated samples, surfactant molecules are present in the pores in their cationic form (CTA^+), since a very low amount of chlorine was detected by elemental analysis.

2.2. Characterizations of Materials. The structural order of synthesized materials was evaluated by powder X-ray diffraction (XRD). Diffraction patterns were recorded at room temperature on a powder PANanalytical X'PERT PRO diffractometer, equipped with a Cu anode ($\lambda_{K\alpha} = 1.5418$ Å, $0.5 < 2\theta < 10°$, 0.02°/s).

After being calcined at 813 K for 6 h and outgassed (1 h at 363 K followed by one night at 573 K), the samples were studied by nitrogen adsorption/desorption measurements on a Micromeritics Tristar 3000 analyzer at 77 K. As-synthesized samples were analyzed too after degassing at 363 K for 24 h. Calculation of the specific surface area was performed by the Brunauer−Emmett−Teller method.[35] Pore diameters and mesoporous volumes were evaluated by the Barrett−Joyner−Halenda method[36] from the desorption branch of the isotherm by use of the Broekhoff−de Boer model.[37,38]

TEM images were collected on a Philips CM200 microscope equipped with a LaB_6 filament. The accelerating voltage was 200 kV. The samples were prepared by depositing several drops of a diluted mesoporous silica suspension in distilled water onto Cu grids coated with a thin (5 nm) holey carbon film.

The organic content of the mesoporous silica samples was determined by thermogravimetry (TG) on a Setaram TG/ATD Labsys thermal analyzer. Dry solid samples were placed in an aluminum oxide crucible and heated from 298 to 1073 K at a heating rate of 5 $K \cdot min^{-1}$ in air.

Elemental analysis of the CTA^+−PBSA encapsulated material was performed by wavelength-dispersive X-ray fluorescence spectroscopy on a Philips MagiX apparatus. Pellets (200 mg) were prepared under 8 tons of pressure.

Stability of the encapsulation of PBSA was studied by dispersing 40 mg of the coencapsulated material in 30 g of an aqueous buffer solution at pH 7 or of ethanol. After 30 min in ethanol and 24 h in both media at 318 K, the mixtures were centrifuged and filtered. The resulting supernatants were analyzed by ultraviolet−visible (UV−vis) spectroscopy. UV−vis spectra were measured in the absorbance mode on a Perkin-Elmer Lambda 35 spectrometer. The amounts of PBSA leached into the supernatants were determined thanks to a calibration curve representing the absorbance at 314 nm as a function of the PBSA concentration. The rate of PBSA leached is equal to the amount of PBSA leached divided by the amount of PBSA introduced. Moreover, the supernatants were also quantitatively analyzed by ^1H NMR on a Bruker Avance 400, after addition of a known quantity of a reference (dioxane) in order to determine the amount of CTA^+ leached.

The ^1H-decoupled ^{29}Si MAS NMR spectra were recorded on a Bruker Avance II 300 WB spectrometer operating at 59.59 MHz ($B_0 = 7.1$ T), with a pulse duration of 2 μs corresponding to a flip angle of $\pi/6$ and a recycle delay of 60 s. Experiments were performed on a standard double-bearing 7-mm Bruker probe head with a spinning frequency of 4 kHz. $^1H-^{29}Si$ frequency-switched Lee−Goldburg heteronuclear correlation (FSLG HETCOR) experiments were performed with a 4-mm probe at a spinning frequency of 12 kHz, with a 4-ms contact time.

$^1H-^{13}C$ cross-polarization magic-angle spinning (CP-MAS) NMR spectra have been recorded on a Bruker Avance II 400WB spectrometer ($B_0 = 9.4$ T) operating at 100.2 MHz. Samples were packed in a 4-mm diameter cylindrical zirconia rotor and spun at a spinning frequency of 10 kHz. $^1H-^{13}C$ CP-MAS NMR experiments were performed with a proton $\pi/2$-pulse duration of 3.2 μs, a contact time of 1 ms, and a recycle delay of 4 s. The dipolar dephasing $^1H-^{13}C$ CP-MAS NMR spectra were recorded with a rotor-synchronized dephasing delay of 40 μs between cross-polarization and decoupling as suggested in the literature for organic solids.[39] $^1H-^{13}C$ FSLG HETCOR experiments were performed at a spinning frequency of 12 kHz, with a 1-ms contact time and two-pulse phase-modulation (TPPM) decoupling during acquisition.

^1H, ^{29}Si, and ^{13}C chemical shifts are given relative to tetramethylsilane (TMS).

Decompositions of the NMR spectra to extract the proportion of the corresponding species were performed with the DMfit software.[40]

3. Results and Discussion

3.1. General Considerations. ***3.1.1. Pore Network Structure.*** XRD pattern of the as-synthesized reference sample shows four broad Bragg reflections that can be indexed as d_{100}, d_{110}, d_{200}, and d_{210} (Figure 1a), which are characteristic of a hexagonal symmetry as expected for MCM-41 type architecture ($a_{hex} = 4.5$ nm).[2]

The diffractogram of PBSA−CTA^+ coencapsulated sample is significantly different. Only one weak and broad reflection at 2.4° 2θ is observed (Figure 1b), indicating the presence of a mesostructuration, which seems to be due to organic matter (vide infra) since the XRD pattern of the calcined coencapsulated

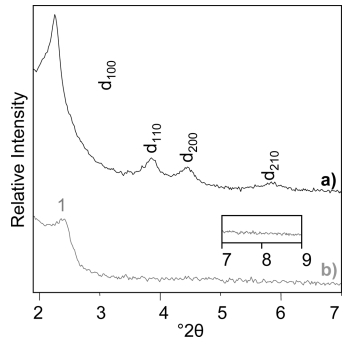

Figure 1. XRD patterns of (a) reference sample and (b) coencapsulated material.

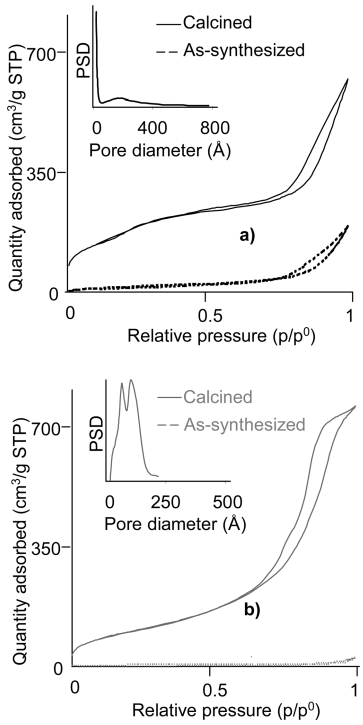

Figure 2. Nitrogen sorption isotherms at 77 K of (a) reference sample and (b) coencapsulated material.

sample does not exhibit any reflection (not shown). Thus, the presence of active molecules perturbs the silicate species/CTAC system in the synthesis medium and consequently the silica network formation, leading to a material without mesoscopic pore arrangement. It is also worth noting the absence of any reflection around 8.6° 2θ (inset, Figure 1), which is characteristic of crystalline PBSA.[29]

3.1.2. Porosity. N_2 adsorption−desorption isotherms of the reference sample and the CTA^+−PBSA coencapsulated material are given in Figure 2. The calcined reference sample isotherm (Figure 2a) is a mixture between types II and IV according to the IUPAC classification.[41] Indeed, type IV is characterized by a small inflection, at relatively low partial pressure (in this case $p/p^0 = 0.2$), indicating the existence of internal secondary micropores. This observation is confirmed by the pore-size distribution (PSD) given in the inset of Figure 2a. Unfortunately, the diameter of these pores cannot be estimated, since their average diameter is smaller than the detection limit of the apparatus ($d = 1.7$ nm). The increase of the adsorbed volume in the high relative pressures region is characteristic of a type II isotherm and indicates the presence of large mesopores, which is probably due to textural porosity. A type II isotherm, with

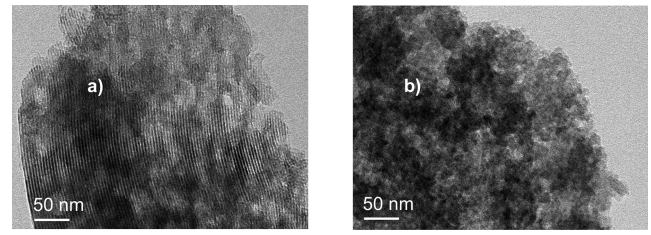

Figure 3. TEM photomicrographs of (a) reference sample and (b) coencapsulated material.

similar increase of the adsorbed volume at high partial pressures and similar hysteresis, was obtained for the as-synthesized reference sample (Figure 2a), which confirms that the presence of large mesopores is due to textural porosity. Thus, in addition to the internal porosity, a textural porosity obviously exists in the reference material. The PSD also confirms the presence of large mesopores, with a large pore-size distribution centered on approximately 18 nm.

The isotherm of the calcined CTA^+−PBSA coencapsulated material (Figure 2b) is of type IV. The increase of the adsorbed volume is observed at high partial pressure ($p/p^0 = 0.75$), indicating the presence of large mesopores. The isotherm of the as-synthesized coencapsulated sample (Figure 2b) is flat, indicating the absence of textural porosity and confirming that the step at high relative pressure observed on the corresponding calcined sample isotherm is due to an internal mesoporosity. In conclusion, organic species are occluded within the pores of the as-synthesized material, entirely filling the porosity.

The PSD of the calcined CTA^+−PBSA coencapsulated material (inset Figure 2b) confirms the absence of secondary microporosity and shows a large pore-size distribution from 2 to 25 nm with two maxima centered on 8 and 12 nm. These results indicate that the coencapsulated material presents a bimodal mesoporosity. Moreover, its BET surface area is smaller than that of the reference sample (410 vs 525 $m^2 \cdot g^{-1}$) but its pore volume is higher (1.1 vs 0.8 $cm^3 \cdot g^{-1}$). These significant structural and textural differences, due to the presence of PBSA in the synthesis medium, suggest that these active molecules interact with the surfactant molecules and the silicate species. Indeed, pore size and organization is mainly governed by surfactant molecules. It is also worth noting that those adsorption data indicate that CTA^+ and PBSA are mainly encapsulated *inside* the pores of the mesoporous silica.

3.1.3. Morphology. Figure 3 shows TEM images of the MCM-41 reference sample and the coencapsulated material. Ordered mesopores structure of the reference sample (Figure 3a) is clearly observed. A granular morphology made of about 40 nm diameter quasispherical particles can be also observed. On the other hand, the coencapsulated sample presents granular morphology with 10 nm diameter quasispherical particles. The porosity of this sample cannot be clearly evidenced by this technique (Figure 3b) since it is disordered, as previously shown by XRD. Moreover, TEM images of the calcined sample (not shown) are similar, which indicates that no textural damage occurs under calcination. The TEM observations suggest that the pores of the coencapsulated sample are delimited by walls made of 10 nm diameter particles.

3.1.4. Chemical and Thermal Analyses. The content of organic species present in the reference sample and in the coencapsulated material was determined by thermogravimetric analysis. Figure 4 shows TG and heat flow curves of both samples during heating in air. In the 25−150 °C temperature range, the removal of physically adsorbed water is observed,

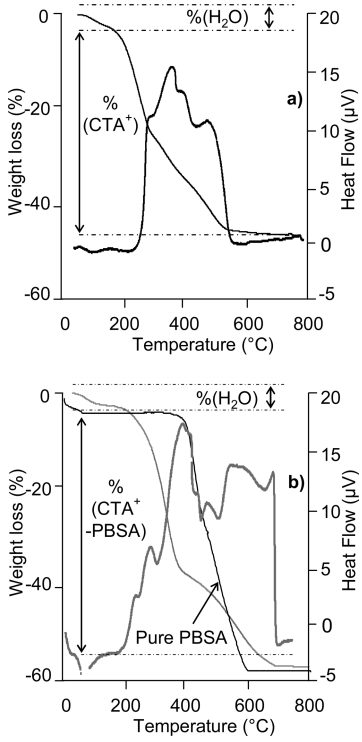

Figure 4. TG and heat flow plots of (a) reference sample and (b) coencapsulated material.

with a weight loss of about 3 wt % for both samples. A second weight loss occurs between 150 and 800 °C, which is mainly due to the decomposition of organic species present in the samples but also to the loss of water due to dehydroxylation. This latter, in minor proportion, will be neglected in the following. For the reference sample (Figure 4a), this second weight loss corresponds exclusively to CTA^+. The mechanism of decomposition of CTA^+ involves three steps.[42] An initial endothermic effect, between 180 and 270 °C, was assigned to Hofmann elimination of trimethylamine, leading to a hydrocarbon chain. The second step, appearing in the temperature range of 270−400 °C, was shown to be exothermic and to originate from a carbon chain fragmentation. Finally, oxidation occurring above 400 °C converted the remaining organic components to carbon dioxide and water. TG data allows determining a total CTA^+ proportion of 44 wt %. Consequently, the reference material is composed of 44 wt % CTA^+, 53 wt % silica, and 3 wt % H_2O.

The weight loss and heat flow curves of coencapsulated material show several differences compared to those of the reference sample (Figure 4b). Except for the loss of physically adsorbed water (3 wt %) that is similar to the reference sample, a weight loss of 60 wt % in the 150−800 °C temperature range, corresponding to the decomposition of the organic matter, was observed. This higher organic content is consistent with the presence of PBSA in the coencapsulated material. A more detailed analysis of TG and differential thermal analysis (DTA) curves shows that the removal of CTA^+ in the coencapsulated material starts at 200 °C, whereas it begins at 180 °C for the reference sample. Moreover, the decomposition of PBSA in the coencapsulated sample finishes at 700 °C, whereas the decomposition of pure PBSA (Figure 4b) takes place from 400 to 600 °C, suggesting that PBSA probably interacts with another constituent of the coencapsulated material. The temperature ranges for the decomposition of CTA^+ and PBSA are overlapping, preventing the discrimination of both organic species according to this technique. In order to determine the proportion of PBSA and CTA^+ in the material, the sulfur content of the sample (characteristic of the sulfonate functionality of the PBSA molecules) was measured by X-ray fluorescence spectroscopy and permitted to determine the PBSA content. Therefore, combination of TG and elemental analysis data allows determination of the final composition of the coencapsulated material, that is, 33 wt % CTA^+, 27 wt % PBSA, 37 wt % silica, and 3 wt % water. Consequently, a weight ratio of 268 mg of PBSA/1000 mg of coencapsulated material (TG weight ratios were corrected by subtracting water) was calculated. The molar ratio PBSA/CTA^+ in the coencapsulated sample is 0.84, which is lower than the one in the synthesis medium (1.38). Consequently, some PBSA molecules were not encapsulated in the mesoporous silica during the synthesis. Indeed, the elemental analysis (by atomic absorption for Si and ^1H liquid state NMR for both CTA^+ and PBSA) of the mother liquor confirmed the presence of PBSA (∼10 mol % relative to the initial amount) and traces (<1 mol % relative to the initial amount) of CTA^+ and Si. Nevertheless, encapsulation of a significant amount of PBSA was achieved.

3.1.5. Stability of Encapsulation. As the properties of the prepared material and thus its applications strongly depend on the stability of the encapsulation, this parameter has been investigated in different solvents. Only 6 wt % of PBSA present in the coencapsulated material was leached after 24 h in a buffer solution at pH 7, whereas no surfactant was detected in the supernatant. Consequently, the largest part of the hydrophilic PBSA molecules is not eliminated from the solid after washing with the buffer solution and tends to confirm that some strong interactions exist between PBSA, CTA^+, and/or the silica network.

The stability of the encapsulation was also investigated in ethanol. After immersion in this solvent for both 30 min and 24 h, it was found that 81 wt % of PBSA and 85 wt % of CTA^+ were leached (corresponding to a PBSA/CTA^+ molar ratio of 0.91). These results are also consistent with the chemical analysis performed on the ethanol-washed materials. Indeed, thermogravimetric analysis shows that 18 wt % of organic species is still present in the ethanol-washed materials (Figure S1, Supporting Information), the latter corresponding approximately to 9 wt % PBSA and 9 wt % surfactant (corresponding to a PBSA/CTA^+ molar ratio of 0.96). As pure PBSA is not soluble in ethanol, the loss of roughly the same amount of PBSA and CTA^+ was attributed to the formation of ethanol-soluble PBSA−CTA^+ aggregates. The presence of such aggregates is not surprising since the good affinity between these two ionic species has already been reported.[43,44] The ethanol-washed sample was analyzed by XRD and, similarly to the calcined sample, the reflection at 2.4° 2θ was not observed. Thus, this reflection present in the as-synthesized sample could be attributed to these ethanol-soluble PBSA−CTA^+ aggregates, which probably form a multilayer arrangement. It is noteworthy that the amount of PBSA and CTA^+ remaining in the solid is the same whatever the immersion time in ethanol (30 min or 24 h), indicating that the encapsulation of these residual organic species is stable in this medium.

The N_2 adsorption−desorption isotherms of the as-synthesized material washed in ethanol are similar to those of the calcined sample (Figure S2, Supporting Information). Washing with ethanol seems to free the internal porosity in the same way as the calcination does. These results seem to indicate that PBSA−CTA^+ aggregates are occluded within the pores of the material. A more detailed analysis of these isotherms shows a

lower BET surface area for the ethanol-washed sample (330 vs 410 $m^2 \cdot g^{-1}$). Moreover, the PSD of the coencapsulated sample washed with ethanol exhibits a single 12 nm diameter pore-size population whereas the calcined material has two types of pores with diameters of 8 and 12 nm. It seems that washing with ethanol delivers only the larger mesopores, whereas the smaller ones are still filled with organic species, which do not form ethanol-soluble PBSA−CTA^+ aggregates. The presence of organic species in the smaller pores explains the lower BET surface area for the ethanol-washed sample, compared to the calcined one. Moreover, these organic species that are not leached in ethanol are probably in strong interaction with the silica framework.

The above characterizations tend to prove that encapsulation of PBSA with a high content was successful. It was also shown by TEM observations, XRD, and porosity measurements that the in situ encapsulation of PBSA has an effect on the silica network formation/organization, probably due to the interactions between PBSA, silicate species, and surfactant molecules in the synthesis medium. Indeed, the coencapsulated material presents a disordered bimodal mesoporosity filled with organic species. The stability tests performed in a buffer solution at pH 7 showed that PBSA molecules strongly interact with CTA^+ molecules and/or silica framework. However, the stability tests performed in ethanol suggest that the larger 12 nm diameter pores are filled with PBSA−CTA^+ aggregates that are soluble in ethanol medium, whereas the smaller 8 nm diameter pores are filled with PBSA and CTA^+ molecules that do not form ethanol-soluble aggregates. These results suggest the existence of different interactions between the components of the material depending on their localization. Indeed, the stability is highly correlated to the localization of the active molecules and also to host−guest interactions. In order to go deeper into the characterization of host−guest interactions and to study in more detail the consequences of encapsulation on each component of the material (PBSA, CTA^+, and silica), a solid-state NMR study was performed. PBSA molecules present several functional groups likely to interact with silanol of the host matrix and/or with the surfactant molecules (CTA^+), which possess a polar headgroup (trimethylammonium cation) and a nonpolar alkyl chain of 16 carbons. It is noteworthy that at the synthesis pH (8.5), the sulfonic acid of PBSA is deprotonated and the amine is protonated, which is favorable for the formation of PBSA−CTA^+ aggregates. Moreover, the protonated amine is a potential hydrogen-bond donor that could interact with the silica host, which is negatively charged. Solid-state NMR will also provide interesting information about the spatial proximity between each component. At this stage, it must be underlined that all NMR experiments were performed at ^{29}Si and ^{13}C natural abundance.

3.2. Solid-State NMR Study. ***3.2.1. ^{29}Si MAS NMR.*** The reference sample and CTA^+−PBSA coencapsulated materials were analyzed by ^{29}Si MAS NMR, which informs about the environment of silicon atoms and consequently about the degree of condensation of silica network. Indeed, the ^{29}Si isotropic chemical shift is strongly dependent on both the nature of neighboring atoms and the number of siloxane bonds around the Si atom.

The ^{29}Si MAS NMR spectra of both samples are presented in Figure 5. Three resonances at about −110, −101, and −91 ppm, corresponding respectively to Q_4 [Si-$(OSi)_4$], Q_3 [Si-$(OSi)_3(OH)$], and Q_2 [Si-$(OSi)_2(OH)_2$] units, are detected for both samples. Decomposition of each spectrum, realized by use of the DMfit software,[40] allows determination of the area of each signal, and hence the proportion of each Q_n ($2 \leq n \leq 4$) type species in both materials. A significantly lower amount of Q_3 (22% vs 30%) and Q_2 (1% vs 5%) species is observed when PBSA is coencapsulated. Accordingly, the proportion of Q_4 species is more important for materials containing PBSA (77%), whereas in the reference sample it accounts for only 65% of the signal. Consequently, these results confirm that coencapsulation of PBSA has an influence on the silica network (as already shown by XRD and porosity measurements), reducing the amount of framework defects such as Q_2 and Q_3 species. Indeed, as shown in the previous section, the major part of the CTA^+ molecules that form ethanol-soluble PBSA−CTA^+ aggregates probably do not interact with silicate species during the formation of the coencapsulated material. Compared to the reference material, this phenomenon could explain the more condensed silica framework observed for the coencapsulated material.

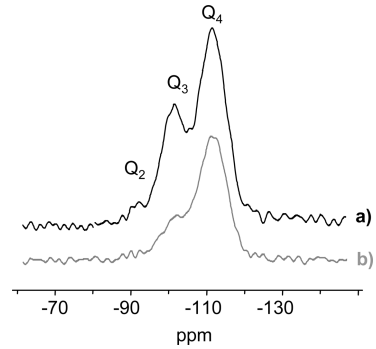

Figure 5. ^1H-decoupled ^{29}Si MAS NMR spectra of (a) reference sample and (b) coencapsulated material.

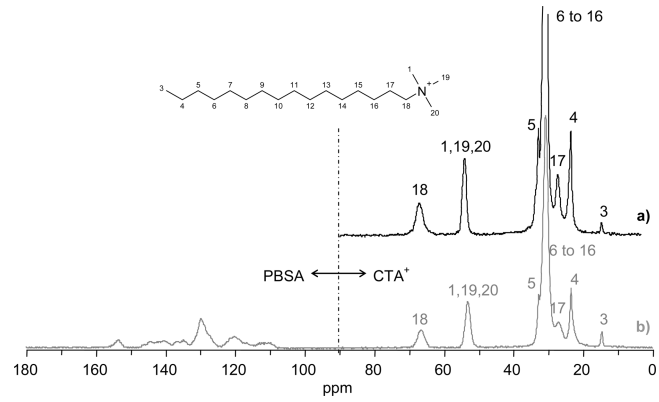

Figure 6. $^1H-^{13}C$ CP-MAS NMR spectra of (a) reference sample and (b) coencapsulated material.

3.2.2. $^1H-^{13}C$ Cross-Polarization Magic-Angle Spinning NMR. $^1H-^{13}C$ CP-MAS NMR is known to provide valuable information about integrity and mobility of organic species,[45] such as PBSA or CTA^+. Figure 6 shows $^1H-^{13}C$ CP-MAS NMR spectra recorded on both mesoporous silica materials. For clarity, the atom numbering of the organic components (CTA^+ and PBSA) is also given in Figures 6 and 7. Well-resolved resonances characteristic of the CTA^+ surfactant molecules are observed in the $^1H-^{13}C$ CP-MAS NMR spectrum of the reference material (Figure 6a) in the 0−70 ppm chemical shift range. Assignment of those resonances reported in Figure 6a is proposed thanks to chemical shift calculation performed with the ACDLab software. Alkyl carbon atoms of surfactant molecules are detected between 20 and 40 ppm, whereas the trimethylammonium polar head is observed at 55 ppm (CH_3) and 67 ppm (N−CH_2).

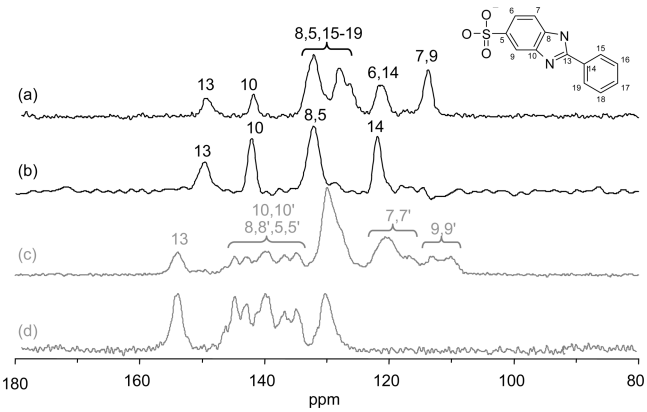

Figure 7. $^1H-^{13}C$ CP-MAS NMR spectra of (a) pure PBSA and (c) coencapsulated material, together with $^1H-^{13}C$ dipolar dephasing CP-MAS NMR spectra of (b) pure PBSA and (d) coencapsulated material.

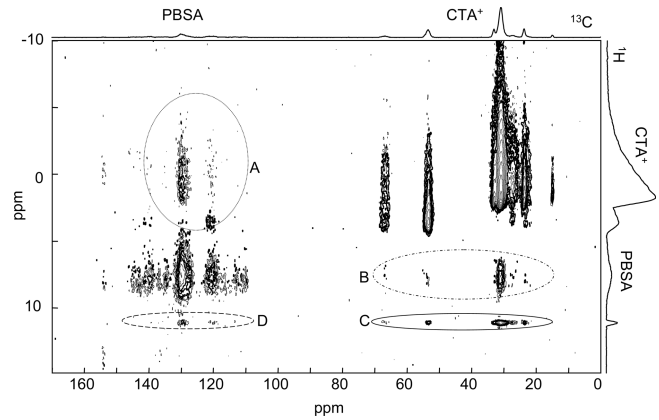

Figure 8. $^1H-^{13}C$ HETCOR spectrum of coencapsulated material.

$^1H-^{13}C$ CP-MAS NMR spectrum of CTA^+-PBSA coencapsulated material presented in Figure 6b exhibits, as expected, the resonances associated with CTA^+ between 0 and 70 ppm, but several differences between the two spectra must be mentioned. Resonances corresponding to the alkyl chain and to the polar head of CTA^+ are significantly broadened, indicating a reduced mobility of CTA^+ when PBSA is coencapsulated. Finally, the resonance corresponding to the $N-CH_2$ (C18) is 2 ppm deshielded, indicating a modification of the environment of this carbon upon encapsulation of PBSA.

The resonances present in the 100−160 ppm chemical shift range are characteristic of aromatic carbon atoms belonging to PBSA molecules. In order to go deeper into the assignment of PBSA resonances and also to evaluate the effect of encapsulation on the PBSA molecules, $^1H-^{13}C$ CP-MAS and dipolar dephasing NMR spectra of pure PBSA were also recorded. The result is displayed in Figure 7a,b, together with an expansion of the 100−160 ppm region of the $^1H-^{13}C$ CP-MAS NMR spectrum of CTA^+-PBSA coencapsulated material (Figure 7c). Comparison of spectra a and c in Figure 7 shows that resonances corresponding to PBSA differ significantly depending on whether the molecule is pure or encapsulated in mesoporous silica, indicating that encapsulation has an effect on the structure of PBSA. Indeed, some resonances present in the 135−145 ppm chemical shift range, but also between 110 and 125 ppm, are split in the spectrum of coencapsulated material compared to the spectrum of pure PBSA. At this stage, it is helpful to assign resonances according to the carbon numbering given in the inset of Figure 7. According to their chemical shifts, the resonances at 149.9 and 142.3 ppm (Figure 7a) are assigned to C13 and C10, respectively. In order to discriminate quaternary carbon (C13, C10, C8, C5, and C14) from CH (C7, C9, C15−19), a $^1H-^{13}C$ CP-MAS dipolar dephasing NMR experiment was performed. Indeed, inserting a small delay without proton decoupling between the CP sequence and the recording of the signal suppresses the CH resonances. The corresponding spectrum shown in Figure 7b confirms the attribution previously suggested for C13 and C10 and indicates that the resonance at 132.3 ppm corresponds to C8 and C5 (which are not resolved) whereas the carbon C14 is detected at 122.2 ppm. Consequently, the resonance at 114.2 ppm detected in the $^1H-^{13}C$ CP-MAS NMR spectrum of pure PBSA must correspond to the CH carbons C7 and C9. Because the resonance at 122.2 ppm in the $^1H-^{13}C$ CP-MAS NMR spectrum of pure PBSA (Figure 7a) is more intense than the ones at 149.9 and 142.3 ppm, it may account for the two carbons C6 and C14. Finally, C15−C19 belonging to the phenyl group are detected at either 132.3 or 128.4 ppm. Once the ^{13}C resonances from pure PBSA have more or less been assigned, it is interesting to compare with the ^{13}C spectrum of PBSA$-CTA^+$ coencapsulated material.

The resonance observed at 150 ppm in the spectrum of pure PBSA and assigned to C13 is significantly shifted in the spectrum of the coencapsulated material (Figure 7c). Such a displacement, of about 4 ppm, indicates a significant variation of the environment of this carbon, suggesting the presence of hydrogen bond between the NH group of PBSA and either CTA^+ or the silica matrix.

Furthermore, when PBSA is coencapsulated, the number and position of C10, C8, C7, and C9 resonances observed in the pure PBSA spectrum are split in the spectrum of coencapsulated material, indicating the coexistence of two forms of PBSA within the coencapsulated material depending on the position of the proton on either N atom of PBSA molecules. Dipolar dephasing NMR experiments (Figure 7d) confirm that the five resonances of relative intensities 1/1/2/1/1 observed between 132 and 146 ppm correspond to quaternary carbons that must be assigned according to their chemical shifts to C10, C5, and C8 in these two forms, while the resonances between 108 and 120 ppm are attributed to carbons 9 and 7 in both environments. This hypothesis is in reasonable agreement with the number of observed resonances and is moreover consistent with the corresponding assignment performed on pure PBSA.

The coexistence of two forms of PBSA may be related to the fact that PBSA is encapsulated in two types of mesopores within the coencapsulated material. These 12 and 8 nm diameter mesopores are respectively filled with ethanol-soluble PBSA$-CTA^+$ aggregates and with PBSA and CTA^+ molecules that do not form ethanol-soluble aggregates. Thus, PBSA must undergo different interaction depending on its localization within the material. In order to prove that the two forms of PBSA are related to their localization in the smaller or larger mesopores, a ^{13}C MAS NMR spectrum of the ethanol-washed material was recorded. Unfortunately, as the amount of PBSA in this material is too low (9 wt %), the signal-to-noise ratio is not good enough to give any reliable conclusion.

In order to focus on the interactions between the different constituents of the coencapsulated mesoporous silica material, that is, silica, CTA^+, and PBSA, $^1H-^{13}C$ and $^1H-^{29}Si$ HETCOR experiments were performed to study the spatial proximity between the three components.

The $^1H-^{13}C$ HETCOR experiment is shown Figure 8 together with the ^1H and ^{13}C projections. As expected, both the ^1H and ^{13}C resonances characteristic of CTA^+ and PBSA are present together with intramolecular H−C correlations. More interesting

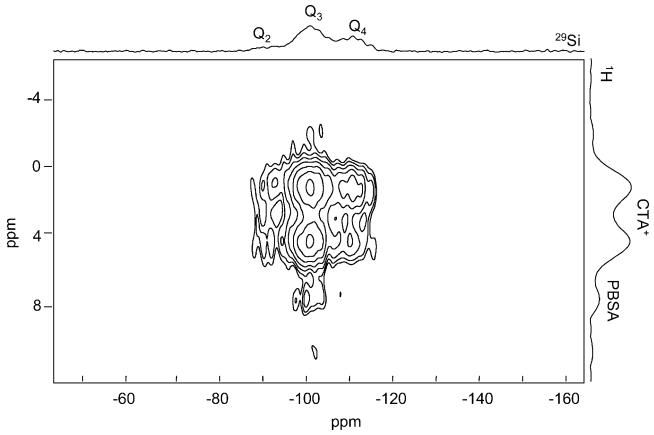

Figure 9. $^{1}H-^{29}Si$ HETCOR spectrum of coencapsulated material.

are the observed $^{1}H-^{13}C$ intermolecular correlations indicating a clear spatial proximity between the protons of the alkyl chain of CTA^+ and the carbon from the phenyl of PBSA (area A in Figure 8) or between the protons belonging to PBSA and carbons of the polar head and the carbon chain of surfactant molecules (area B in Figure 8). The presence of these intermolecular correlations proves that these two molecules are spatially closed, in agreement with the stability results that suggest the formation of $PBSA-CTA^+$ aggregates. More precisely, it is interesting to note the absence of any correlation between PBSA and the terminal methyl of the alkyl chain of CTA^+, while the aromatic carbons of PBSA are correlated with the methyl groups of the polar head and with some CH_2 of the carbon chain of CTA^+. Presumably, PBSA is placed close to the polar head of the surfactant within the mesoporous silica, which is also consistent with the fact that PBSA is a hydrophilic molecule.

In addition, a fine resonance is observed at 13 ppm in the ^{1}H dimension, which could correspond to the NH groups of PBSA as this resonance is also detected in the ^{1}H MAS NMR spectra of pure PBSA but not in that of reference material (spectra not shown). This resonance is correlated with both the polar head and CH_2 groups of the surfactant but not with the terminal CH_3 groups (area C in Figure 8) and is also correlated with the aromatic rings of PBSA (area D in Figure 8). This spatial proximity strongly suggests an interaction between the polar head of the surfactant and PBSA through the amine groups, which is precisely the structure of the $PBSA-CTA^+$ aggregates inside the mesoporous silica material. In this case, the schematic model of interdigitated $PBSA-CTA^+$ bilayers suggested in the literature is not valid.[43,44]

$^{1}H-^{29}Si$ HETCOR experiments performed on the coencapsulated mesoporous silica sample (Figure 9) displayed clear correlations between the proton of the surfactant molecules at 1.2 and 4.2 ppm and the Q_2, Q_3, and Q_4 silicon signals from the matrix. Furthermore, a unique correlation is also detected between the proton (7.3 ppm) characteristic of aromatic protons from the PBSA molecules and Q_3 species from the mesoporous silica framework. Consequently, as already suspected from 1D ^{29}Si MAS NMR, the hydrophilic active molecules of PBSA are also interacting with silanol of the inorganic framework, which may explain the remarkable stability of PBSA encapsulation in this material in hydrophilic media.

4. Conclusion

CTA^+-PBSA coencapsulated mesoporous silica materials were synthesized by the in situ method. The reported characterizations of this material allow us to conclude that the high amount of PBSA encapsulated (27 wt %) is occluded within the mesopores of the silica host. Moreover, the presence of PBSA has an effect on the structure and texture of the material, probably due to the interactions between PBSA, silicate species, and surfactant molecules in the synthesis medium. Despite the use of an MCM-41 protocol, the coencapsulated material presents a disordered bimodal mesoporosity, in which the active molecules and the surfactant undergo different interactions according to their localization. Indeed, the larger pores are filled with $PBSA-CTA^+$ aggregates that are soluble in ethanol medium, whereas the smaller ones are filled with PBSA and CTA^+ molecules that do not form ethanol-soluble aggregates. Thanks to solid-state NMR spectroscopy, an overall picture of the organic/inorganic interface can be suggested as shown in Scheme 1. The active molecules are shown to interact with both

SCHEME 1: Tentative Description of the Interface between PBSA, CTA^+, and the Silica Matrix

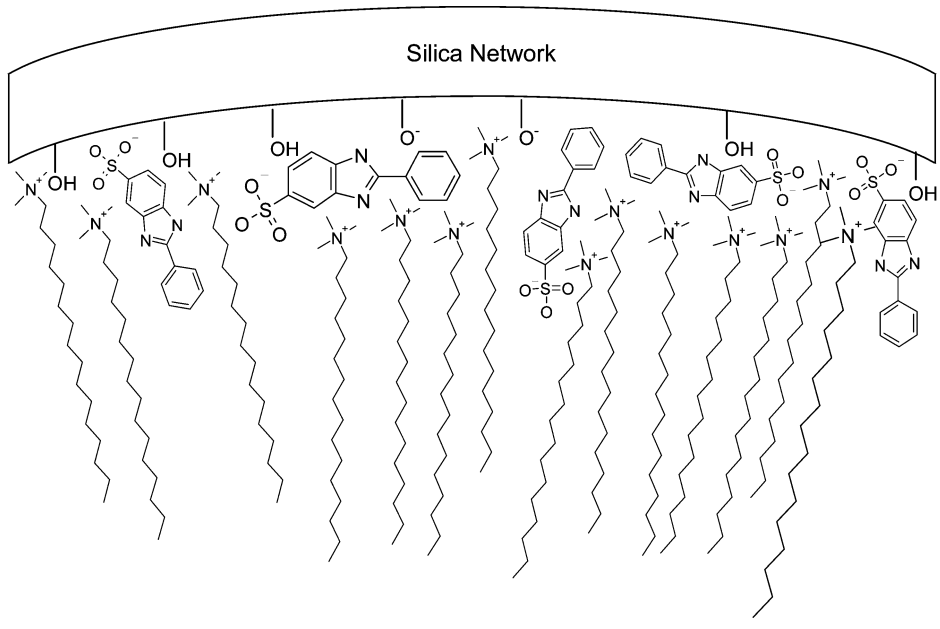

the mesoporous silica host through the silanol groups and with the surfactant molecules, preferentially through their polar head. These "multiple" interactions have interesting consequences on the stability of PBSA encapsulation. Especially, a slower release of the active molecules in hydrophilic media ensures safer and long-lasting sun protection.

Acknowledgment. Dr. Didier Le Nouen, Dr. Loïc Vidal, and Mrs. Laure Michelin are warmly thanked for fruitful discussions, TEM observations and X-ray fluorescence spectroscopy measurements, respectively.

Supporting Information Available: Two figures showing TG and heat flow plots and nitrogen sorption isotherms of the coencapsulated material after 24 h in ethanol. This material is available free of charge via the Internet at http://pubs.acs.org.

References and Notes

(1) Vartuli, J. C.; Beck, J. S. *Nature* **1992**, *359*, 710–712.
(2) Beck, J. S.; Vartuli, J. C.; Roth, W. J.; Leonowicz, M. E.; Kresge, C. T.; Schmitt, K. D.; Chu, C. T. W.; Olson, D. H.; Sheppard, E. W.; McCullen, S. B.; Higgins, J. B.; Schlenker, J. L. *J. Am. Chem. Soc.* **1992**, *114*, 10834–10843.
(3) Moller, K.; Bein, T. *Chem. Mater.* **1998**, *10*, 2950–2963.
(4) Hartmann, M.; Pöppl, A.; Kevan, L. *J. Phys. Chem.* **1995**, *99*, 17494–17496.
(5) Ryoo, R.; Ko, C. H.; Kim, J. M.; Howe, R. *Catal. Lett.* **1996**, *37*, 29–33.
(6) Böhlmann, W.; Schandert, K.; Pöppl, A.; Semmelhack, H. C. *Zeolites* **1997**, *19*, 297–304.
(7) Worboys, L. M.; Edward, P. P.; Anderson, P. A. *Chem. Commun.* **2002**, 2894–2895.
(8) Sano, T.; Oumi, Y. *Catal. Surv. Asia* **2004**, *8* (4), 295–304.
(9) Valsesia, P.; Beretta, M.; Bracco, S.; Comotti, A.; Sozzani, P. *J. Mater. Chem.* **2008**, *18*, 5511–5517.
(10) Langer, R. *Nature* **1998**, *392*, 5–10.
(11) Park, K. *Controlled Drug Delivery: Challenges and Strategies*; American Chemical Society: Washington, DC, 1997.
(12) Fujii, T.; Ishii, A.; Anpo, M. *J. Photochem. Photobiol. A* **1990**, *54* (2), 231–237.
(13) Clifford, N. W.; Swaminathan Iyer, K.; Raston, C. L. *J. Mater. Chem.* **2008**, *18*, 162–165.
(14) Charnay, C.; Bégu, S.; Tourné-Péteilh, C.; Nicole, L.; Lerner, D. A.; Devoisselle, J. M. *Eur. J. Pharm. Biopharm.* **2004**, *57*, 533–540.
(15) Ernst, S.; Gläser, R.; Selle, M. In *Progress in Zeolite and Microporous Materials*; Chon, H., Ihm, S.-K., Uh, Y. S., Eds.; Studies in Surface Science and Catalysis, Vol *105*; Elsevier: Amsterdam, 1997; 1021−1028.
(16) Ernst, S; Selle, M. *Microporous Mesoporous Mater.* **1999**, *27*, 355–363.
(17) Hoppe, R.; Schulz-Ekloff, G.; Wöhrle, D.; Shpiro, E. S.; Tkachenko, O. P. *Zeolites* **1993**, *13*, 222–228.
(18) Brauchle, C. In *Zeolite Chemistry and Catalysis*; Jacobs, P. A., Jaeger, N. I., Kubelkova, L., Wichterlova, B., Eds.; Studies in Surface Science and Catalysis, Vol. 69; Elsevier: New York, 1991.
(19) Ehrl, M.; Kindervater, H. W.; Deeg, F. W.; Bräuchle, C.; Hoppe, R. *J. Phys. Chem.* **1994**, *98*, 11756–11763.
(20) Gfeller, N.; Calzaferri, G. *J. Phys. Chem. B* **1997**, *101*, 1396–1408.
(21) Sutra, P.; Brunel, D. *Chem. Commun.* **1996**, 2485–2486.
(22) Rao, Y. V. S.; Vos, D. E.; Bein, T.; Jacobs, P. A. *Chem. Commun.* **1997**, 355–356.
(23) Macario, A.; Moliner, M.; Corma, A.; Giordano, G. *Microporous Mesoporous Mater.* **2009**, *118*, 334–340.
(24) Ren, T.-Z.; Yuan, Z.-Y.; Su, B.-L. *Colloids Surf., A* **2007**, *300*, 88–93.
(25) Tan, G.; Ford, C.; John, V. T.; He, J.; McPherson, G. L.; Bose, A. *Langmuir* **2008**, *24*, 1031–1036.
(26) Inbaraj, J. J.; Bilski, P.; Chignell, C. F. *Photochem. Photobiol.* **2002**, *75*, 107–116.
(27) Hayden, C. G.; Roberts, M. S.; Benson, H. A. E. *Aust. N.Z. J. Med.* **1998**, *28*, 639–646.
(28) Perioli, L; Ambrogi, V.; Rossi, C.; Latterini, L.; Nocchetti, M.; Costantino, U. *J. Phys. Chem. Solids* **2006**, *67*, 1079–1086.
(29) Scalia, S.; Molinari, A.; Casolari, A.; Maldotti, A. *Eur. J. Pharm. Sci.* **2004**, *22*, 241–249.
(30) Paul, G.; Steuernagel, S.; Koller, H. *Chem. Commun.* **2007**, 5194–5196.
(31) Ma, H.; He, J.; Evans, D. G.; Duan, X. *J. Mol. Catal. B:Enzym.* **2004**, *30*, 209–217.
(32) Ibarra, I.; Loera, S.; Laguna, H. *Chem. Mater.* **2005**, *17*, 5763–5769.
(33) Azaïs, T.; Tourné-Péteilh, C.; Aussenac, F.; Baccile, N.; Coelho, C.; Devoisselle, J.-M.; Babonneau, F. *Chem. Mater.* **2006**, *18*, 6382–6390.
(34) Voegtlin, A. C.; Matijasic, A.; Patarin, J.; Sauerland, C.; Grillet, Y.; Huve, L. *Microporous Mater.* **1997**, *10*, 137–147.
(35) Brunauer, S.; Emmett, P. H.; Teller, E. *J. Am. Chem. Soc.* **1938**, *60*, 309–319.
(36) Barrett, E. P.; Joyner, L. G.; Halenda, P. P. *J. Am. Chem. Soc.* **1951**, *73*, 373–380.
(37) Broekhoff, J. C. P.; de Boer, J. H. *J. Catal.* **1967**, *9*, 15–27.
(38) Broekhoff, J. C. P.; de Boer, J. H. *J. Catal.* **1968**, *10*, 377–390.
(39) Witt, J.; Fenzke, D.; Hoffmann, W. D. *Appl. Magn. Reson.* **1992**, *3*, 151–163.
(40) Massiot, D.; Fayon, F.; Capron, M.; King, I.; LeCalvé, S.; Alonso, B.; Durand, J.-O.; Bujol, B.; Gan, Z.; Hoatson, G. *Magn. Reson. Chem.* **2002**, *40*, 70–76.
(41) Sing, K. S. W.; Everett, D. H.; Haul, R. A. W.; Moscou, L.; Pierotti, R. A.; Rouquerol, J.; Siemieniewska, T. *Pure Appl. Chem.* **1985**, *57*, 603–619.
(42) Kleitz, F.; Schmidt, W.; Schüth, F. *Microporous Mesoporous Mater.* **2003**, *65*, 1–29.
(43) Horbaschek, K.; Hoffmann, H.; Thunig, C. J. *J. Colloid Interface Sci.* **1998**, *206*, 439–456.
(44) Gräbner, D.; Zhai, L.; Talmon, Y.; et al. *J. Phys. Chem.* **2008**, *112*, 2901–2908.
(45) Babonneau, F.; Yeung, L.; Steunou, N.; Gervais, C.; Ramila, A.; Vallet-Regi, M. *J. Sol-Gel Sci. Technol.* **2004**, *31*, 219–223.

JP907051F